

## **Novel Computer Aided Diagnostic System Using Synergic Deep Learning Technique for Early Detection of Pancreatic Cancer**

**Sabah Khudhair Abbas**

Department of Computer Engineering Techniques, Imam Al-Kadhumi University College, Najaf, Iraq.

E-mail: sf18nj@alkadhumi-col.edu.iq

**Rusul. Sabah. Obied**

Department of Educational Planning, General Directorate Education in Najaf, Iraq.

E-mail: Rusulsabah7@gmail.com

*Received February 17, 2021; Accepted June 14, 2021*

*ISSN: 1735-188X*

*DOI: 10.14704/WEB/V18SI02/WEB18105*

---

### **Abstract**

Pancreatic cancer (PC) in the more extensive sense alludes to in excess of 277 distinct kinds of cancer sickness. Researchers have recognized distinctive phase of pancreatic cancers, showing that few quality transformations are engaged with cancer pathogenesis. These quality transformations lead to unusual cell multiplication. Therefore, in this study we propose a Computer Aided Diagnosis (CAD) system using Synergic Inception ResNet-V2, Deep convoluted neural network architecture for the identification of PC cases from publically Usable CT images that could extract PC graphical functionality to include clinical diagnosis before the pathogenic examination, saving valuable time for disease prevention. Simulation results using MATLAB is shown to illustrate that quite promising results have been obtained in terms of accuracy in detecting patients infected with BC. Accuracy of 99.23 per cent is reached using the proposed deep learning method, which is better than all other state-of-the-art approaches available in the literature. The calculation time was found to be less than the other current 22 second process. The proximity of the suggested approach to the True Positive values in the ROC curve suggests a result that is greater than the other methods. The comparative study with Inception ResNet-V2 is based on separate test and training data at a rate of 90 percent-10 percent, 80 percent-20 percent and 70 percent-30% respectively, which shows the robustness of the proposed research work. Experimental findings show the proposed reliability of the device relative to other detection approaches. The proposed CAD device is fully automated and has thus proved to be a promising additional diagnostic tool for frontline clinical physicians.

### **Keywords**

Pancreatic Cancer (PC), Computer Aided Diagnosis (CAD), Synergic Deep Learning.

## **Introduction**

Stages of cancer are divided on the basis of metastasis. Depending on the symptoms and rate of metastasis, there are different sizes to determine different stages. Mainly cancer stages are divided into four parts:

**Stage 1:** Stage 1 of pancreatic cancer involves the expansion of lymph nodes. This is due to the sudden increase in the number of lymphocytes. The risk is minimal at this stage as the cancer has not spread or affected any other organs.

**Stage 2:** Pancreatic Cancer in stage 2, the spleen, liver and lymph nodes are enlarged. It is not necessary that all these elements suffer at once; however, at this stage one of these elements is definitely involved. The growth of lymphocytes in this stage is very high.

**Stage 3:** Pancreatic Cancer in stage 3, anemia develops in stage 3 and the organs mentioned above are even larger. Ensure that more than two elements of the platform are affected.

**Stage 4:** Pancreatic Cancer Stage 4 is the last stage with the highest risk rate. The rate of pancreatic platelets begins to decline rapidly. Cancer cells begin to affect the lungs, including other organs that have already begun to affect them. Anemia, in this case, can be severe.

## **1. Motivation**

The original benefit of this research was the development of CBC's analysis software as a tool for clinical Pancreatic testing, which enables high-quality testing and the ability to automate pancreatic slide images to generate the data needed for diagnosis. This work focuses on standard pancreatic test samples (Chen, Xu, Yiqun Hu and et al 2019). The purpose of this study is to decide if the proposed techniques of image processing are successful in administering the CBC test, especially in the presence of low-quality models. We are particularly interested in classifying five major types of white pancreatic cells (leukocytes) and counting normal red Pancreatic cells (erythrocytes) in the clinical setting.

## **Literature Survey**

An approach for color image enhancement based on fast hue and range preserving histogram (Chang, Hang and et al 2013). It preserves the hue and ranges of red, green and blue channel. At first, the target intensity image is generated from the input image by matching the intensity channel of the RGB 41 image into a specified histogram. Finally, enhanced RGB image is computed based on the target from the stretched image that

satisfies the hue and gamut constraints (Nashwan Jasim Hussein and et al 2017). Partial differential equation algorithm based color image enhancement is analyzed. A shock filter is designed based on single vectors of all components of the input image (Gurcan, Metin and et al 2009). It produces selective smoothing that reduces the noise efficiently and the edges are sharpened. Local processing based image enhancement is presented by Grimier and Lee for color images. The given RGB image is transformed into HSV color space. Two types of enhancements; non-linear transformation and local processing using neighborhood pixels are applied to the luminance channel only for image enhancement (Jiang Huiyan, and et al 2009 and Pahari, Purbanka 2017). Global HE based color image enhancement is described. Initially, each component of given RGB image is processed by global HE method. Then, wavelet transform is applied for original and equalized RGB image (Reddy, C. Kishor Kumar 2015). The detail coefficients of the original RGB image are 46 replaced by the equalized RGB image. Subsequently, wavelet reconstructed image and original images are fused together to compute the enhanced RGB image (Zhou, Yin ad et al 2014). Adaptive filter based color image enhancement approach is consisting of three modules. Initially, the original RGB image is converted into YUV color space. The luminance image is obtained by Y (luma) component and background image is obtained by applying adaptive filter on U and V (color) component respectively (Zhou, Jian, and Olga G 2015). Subsequently, cumulative distribution function based adaptive adjustment is taken place on the luminance and the obtained background image. Finally, linear color image restoration is performed to get enhanced color image (Xu, Yan and et al 2014). Jiang and He implemented a color image enhancement scheme based on a sparse representation (Wang, Jinhua and et al 2016). In order to produce improved color image, the RGB image is initially converted into a Lab color space followed by a DCT decomposition. The amplitudes of the DCT can differ greatly in the edges rather than the texture contents. The effect of textures is also minimized by the use of a certain threshold in the DCT coefficients (Moschopoulos and et al 2013, Finally, Zhang and et al 2020). Texture and edge regions are improved by adding 5-007-power calculation to non-zero coefficients in medium and high-frequency domains and using the Kaiser Window block effects feature to eliminate them (Nashwan Jasim Hussein and et al 2015). A histogram approach for color image enhancement using luminance and contrast enhancement. RGB input image is converted into HSI color space at the start of the enhancement process (Liu, Liangliang and et al 2020). Only the Saturated channel is further used for histogram equalization on each region. Finally, the enhanced RGB is obtained from the enhanced saturation and the untreated hue and intensity components (Shi, Yu Shen and Hwang 2020). Propose a retinex solution to improve the color images. In order to resolve the color shift problem, the given RGB image is converted to HSV color space, while the

value channel is only considered for further processing (Haque, Intisar Rizwan I., and Jeremiah Neubert. 2020). Then, in order to eliminate hallow artifacts, an improved envelope with a gradient-dependent weighting solution is implemented, which reduces disruptions around differences in intensity, such as edges and corners (Chen, Xu 2019, Nashwan Jasim Hussein 2021). Various color space conversions are reviewed for color image enhancement. Eight most common color spaces such as RGB, YCbCr, YUV, YDbDr, HSV, HSI, XYZ, CIELAB, CIELUV, and CIELCH are analyzed with various multi resolution analyses such as wavelet and Contour let transformation (Kurbanov, S.K., and S.S. Beknazarova 2020, Saito, Atsushi 2016). The performances of these approaches are compared by computing conversion accuracy and similarity measure. On account of image enhancement neural network algorithm named ratio rule is adopted to pre and 48 post-processing in the harmonic system. It improves both color rendition and dynamic range compression of the image (Saito, Atsushi and et al 2017).

## **Proposed Methodology**

This section mainly concentrates on this novel application of red Pancreatic cell tumor classification PCCD dataset images are consider which includes both benign and malignant stage sample images (Nashwan Jasim Hussein 2020). The proposed methodology of the system and their algorithms are briefly explained in this chapter. Each and every step of image processing, a new algorithm is implemented with the help of the chapter 2 survey. Moreover, the stages involved in the research work are also discussed. The database used for this proposed work is also explained in detail.

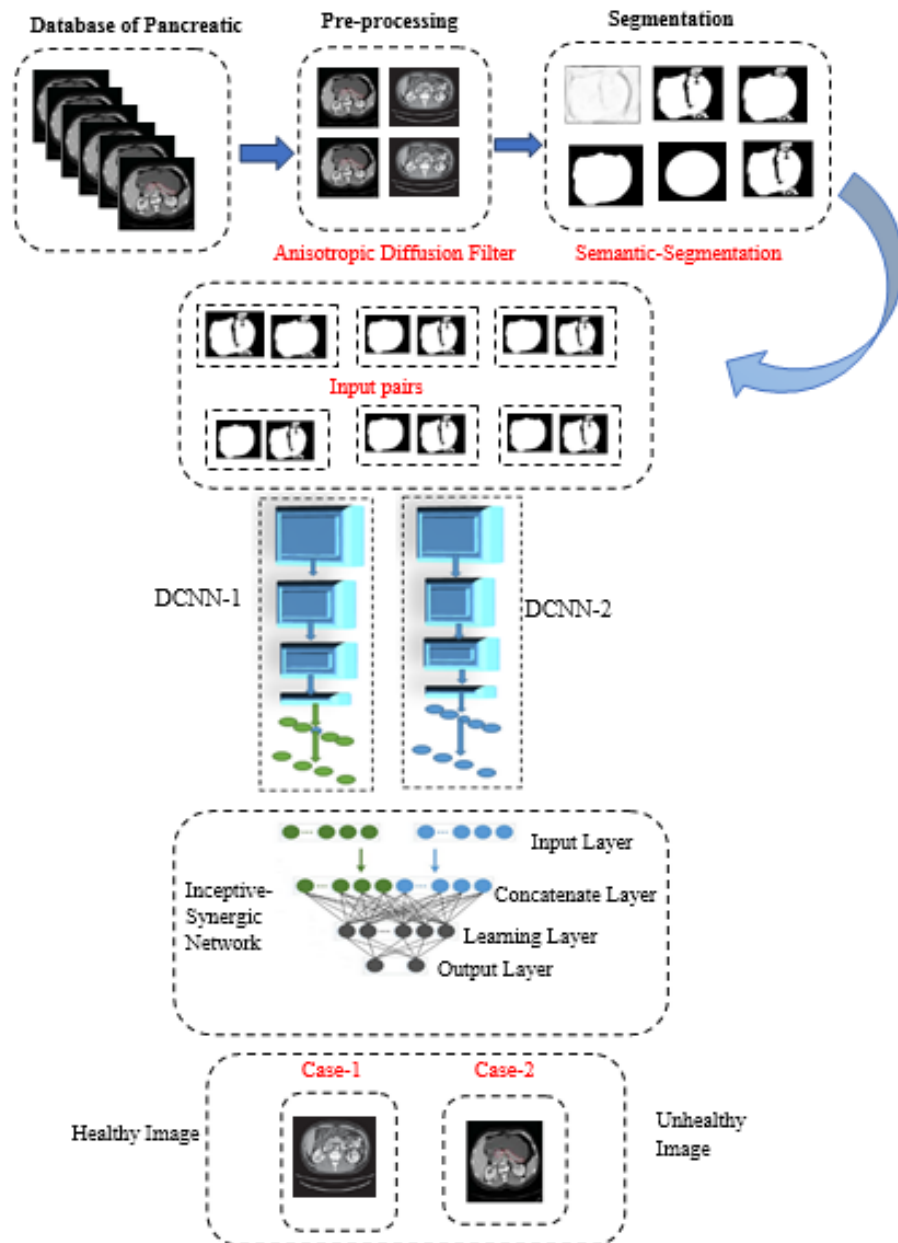
## **Data Base**

The suggested method uses the PCCD dataset (Pancreatic Cell Images dataset) with pancreatic samples of 200 healthy and 200 malignant images of 534 Pancreatic Cell Patients (JPEGs) and their corresponding cell type names (Rosow, David and et al 2012). Eosinophil, Lymphocyte, Monocyte and Neutrophil are four forms of pancreatic cells. These images are then sent to be further analyzed for the identification of cancer cells from normal cells.

## **Block Diagram**

This section discusses mainly about for red pancreatic cells. Pre-processing an image is an essential process for every classification since it makes the image ready for further steps. Initially the Pancreatic sample CT scan image RGB color images are converted into HSV image for the process to be simple. Preprocessing techniques using color conversion and

anisotropic diffusion filter. After the pre-processing level, the performance of this step is given to the segmentation techniques used to remove the cancerous area from CT images (Nashwan Jasim Hussein 2020). Segmentation techniques using proposed semantic segmentation. Classification technique using Deep Learning with feature extraction. The classification of tumor cells is done with features derived from the pancreatic test. The image classification criteria involve train values and testing datasets. At Each image of dataset refers to the multiple featuring values and classification with the attributes.



**Algorithm 1: Semantic Segmentation (SS)**

**Step 1: Input Image Initialization Process**

//\*\*\*\*\* Initialize cluster center  $C_k = [L_k, a_k, b_k, x_k, y_k]^T$  in the hexagonal grid, pixels label matrix  $l$ , distance matrix  $D$  from pixels to cluster centers, hexagonal grid spacing  $S$  and radius  $r$  of circular structure element \*\*\*\*\*//

**Step 2: Move Cluster center**

//\*\*\*\*\*initial cluster center to the smallest gradient position in the hexagonal region.\*\*\*\*\*//

**Step 3: Repeat Process**

//\*\*\*\*\*Repeat the same condition\*\*\*\*\*//

**While** residual error  $\geq$  threshold  $E$  do

//\*\*\*\*\* If the residual error greater than or equal to threshold Do the for condition\*\*\*\*\*//

**For** each cluster center  $C_k$  do

Obtain sub image cluster center & Distance calculation process

//\*\*\*\*\*Obtain sub images (use  $[x_k, y_k]$  as the center,  $2*S$  as the side) containing cluster centers. Calculate the distance between each pixel in the sub image and cluster center. If the distance is less than the previous value, then update its  $l$  and  $D$ \*\*\*\*\*//

End for // \*\*\*\*\*End the for condition\*\*\*\*\*//

Update the cluster center

//\*\*\*\*\* calculate the mean of [equation 1]  $L$ ,  $a$ ,  $b$ ,  $x$  and  $y$  of each super pixel to update the cluster center. Recalculate the residual error, go to the third step, and continue the execution\*\*\*\*\*//

End while // \*\*\*\*\*End the While condition\*\*\*\*\*//

**Step 4: Mask Prediction Process**

//\*\*\*\*\*Obtain all non-connected regions of the MRI image and then perform the open operation of the circular structure element radius  $r$ . The final result is subtracted from the original MRI image denoted as mask \*\*\*\*\*//

**Step 5: Perform distance transform**

//\*\*\*\*\*Perform distance transform on mask, and assign each small region to the nearest super pixel \*\*\*\*\*//

**Step 6: Computation Process**

//\*\*\*\*\*Compute the super pixel adjacency matrix for subsequent operation. Until all CT image sequences are segmented\*\*\*\*\*//

**Step 7: Obtained Output.**

//\*\*\*\*\*Execute connection operations and sequential output\*\*\*\*\*//

## Results and Discussion

The proposed CAD framework is being applied with the aid of MATLAB 2018a tools. The MATLAB code is incorporated in the mathematical and image processing software. 200 healthy and 200 malignant photographs from 534 patients are retrieved from the PCCD archive and examined to achieve the segmentation and classification findings of the proposed method. The following steps show the findings obtained by giving the original CT image of the Pancreatic Cell Tumor from the database. Pre-processing methods are applied to the reference images to eliminate noise and increase the accuracy of the images. This move is followed by segmenting the area of the tumor from the image. The corresponding features derived from the sample images are shown in the table below. Finally, the differentiation step is used to assess the benign or malignant tumor.

### Sample Image

Figure.5.1 displays the reference datasets from the PCCD. Some tests are taken to prove that they have been used to analyze the performance of the proposed device. Some samples of Pancreatic Cell CT are presented below:

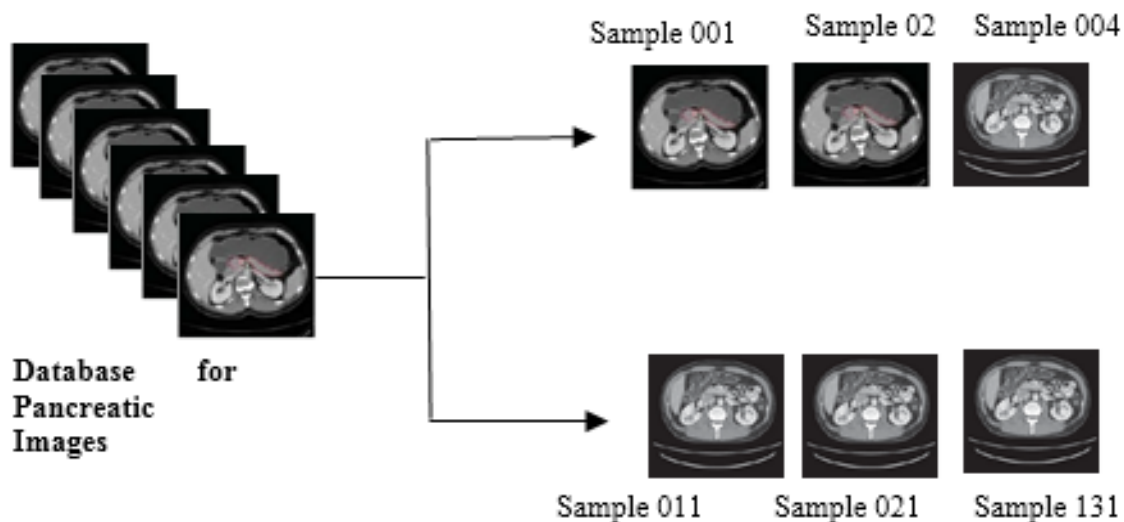


**Figure 5.1 Pancreatic Dataset Samples**

### Proposed Pre-processing

Pre-processing an image is an essential process for every classification since it makes the image ready for further steps. Initially the Pancreatic sample CT scan image RGB color images are converted into HSV image for the process to be simple.



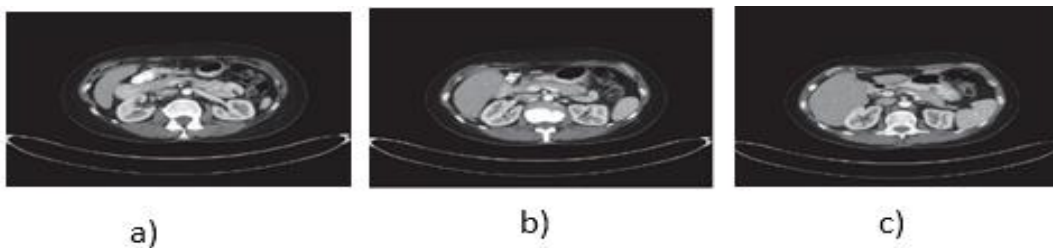


**Figure 5.2 Simulation images for pre-processed Pancreatic Dataset Samples**

Anisotropical filter is utilized to obtain the better results, which adjust image intensities to enhance contrast of both background and foreground. Final enhanced image contains better visual quality and nodules are clearly visible for segmentation process.

**Table 5.1 Pre-processing Performance Metrics**

| Metrics | Anisotropic Filter | Bilateral Filter | Proposed method |
|---------|--------------------|------------------|-----------------|
| PSNR    | 26.56              | 30.68            | <b>35.92</b>    |
| SSIM    | 0.7823             | 0.8453           | <b>0.9125</b>   |
| MSE     | 0.0044             | 0.0028           | <b>0.00052</b>  |

### Image Segmentation

After the stage of pre-processing, the output from this step is given to the segmentation techniques to extract the cancerous region from the CT images. The proposed semantic segmentation is used by finding the minimum area threshold values based on the prior information of the image captured sequence. It is used to enlarge the boundary of the region in the foreground pixels. The image can be segmented according to the shape and characteristics of the image.

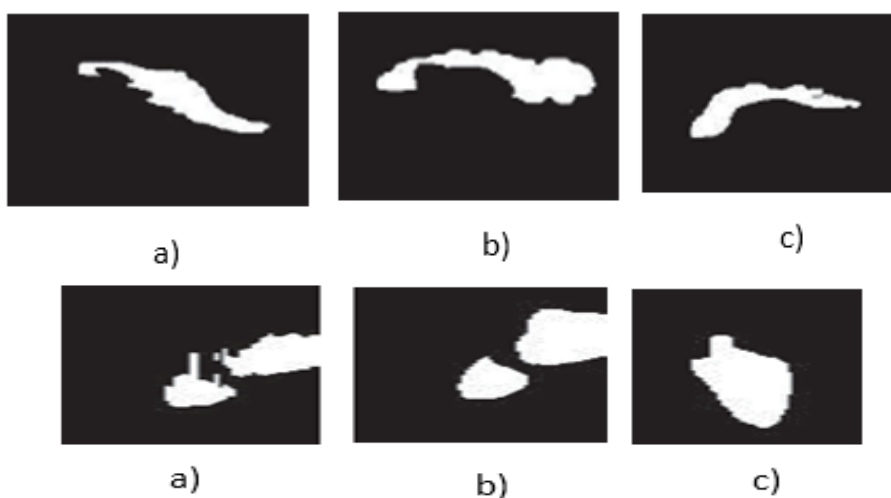


**Figure 5.3 Shows the segmented results of PCCD benign and malignant Pancreatic Cell tumor samples of proposed system**



**Feature Extraction**

For feature extraction, Histogram based features are mainly considered where the feature values mainly depend on the threshold part of the histogram based values. By these features, classifier classifies the disease in the lung image. The histogram can be generated in order to obtain the feature in Histogram based features. For Deep learning ResNet-50 inceptive synergic network classifier provides efficient classification where the features can be extracted. Here, taken 200 images for testing purpose which includes both benign and malignant stages of database images. From these database images, Histogram based features are extracted.

**Table 5.3 Feature Values of Benign Red Pancreatic Cell Tumor CT images**

| Image | Contrast | Cluster Shade | Cluster prominence | Correlation | Dissimilarity | Probability |
|-------|----------|---------------|--------------------|-------------|---------------|-------------|
| 1     | 0.453402 | -24.35896     | 324.884            | 0.928544    | 0.364405      | 0.1952      |
| 2     | 0.480787 | -23.97541     | 369.751            | 0.748975    | 0.201361      | 0.1544      |
| 3     | 0.278814 | -22.28947     | 270.458            | 0.926434    | 0.160338      | 0.1613      |
| 4     | 0.425737 | -23.97845     | 296.354            | 0.954037    | 0.193531      | 0.1643      |
| 5     | 0.482967 | -24.82447     | 332.154            | 0.849975    | 0.241061      | 0.1944      |
| 6     | 0.581298 | -18.94672     | 271.394            | 0.827944    | 0.173282      | 0.1552      |
| 7     | 0.491035 | -19.35874     | 264.897            | 0.754218    | 0.343656      | 0.1653      |
| 8     | 0.407573 | -17.94246     | 279.365            | 0.955328    | 0.475228      | 0.1797      |
| 9     | 0.496626 | -14.75612     | 256.684            | 0.751768    | 0.203421      | 0.1861      |
| 10    | 0.595226 | -16.38726     | 222.333            | 0.959457    | 0.348617      | 0.1883      |
| 11    | 0.241714 | -21.36726     | 278.394            | 0.824956    | 0.244935      | 0.1651      |
| 12    | 0.597532 | -18.97521     | 284.654            | 0.913457    | 0.396749      | 0.1766      |
| 13    | 0.523191 | -22.97564     | 345.897            | 0.745301    | 0.427157      | 0.1842      |
| 14    | 0.579228 | -24.36994     | 336.655            | 0.915996    | 0.271558      | 0.1518      |
| 15    | 0.496519 | -19.06789     | 397.254            | 0.810656    | 0.378492      | 0.1371      |

**Table 5.4 Histogram based features of Benign Red Pancreatic Cell Tumor CT images**

| Image | Mean     | Standard deviation | Skewness | Kurtosis | Entropy  |
|-------|----------|--------------------|----------|----------|----------|
| 1     | 0.023222 | 0.023847           | 3.650224 | 22.51101 | 2.283453 |
| 2     | 0.025319 | 0.036517           | 4.313795 | 18.38667 | 2.214566 |
| 3     | 0.027222 | 0.025593           | 5.754522 | 34.53797 | 2.124188 |
| 4     | 0.021398 | 0.036374           | 4.218666 | 18.46232 | 2.369142 |
| 5     | 0.026492 | 0.035517           | 4.112795 | 17.38067 | 2.214777 |
| 6     | 0.028277 | 0.022263           | 5.257145 | 33.69795 | 2.123543 |
| 7     | 0.021394 | 0.026485           | 4.533173 | 20.49361 | 2.265544 |
| 8     | 0.023256 | 0.033045           | 4.488421 | 24.59704 | 2.406939 |
| 9     | 0.026134 | 0.034398           | 4.225914 | 19.55556 | 2.311871 |
| 10    | 0.024391 | 0.034332           | 4.208308 | 22.41359 | 2.214116 |
| 11    | 0.022477 | 0.022312           | 4.641366 | 21.91316 | 2.359479 |
| 12    | 0.021739 | 0.022031           | 4.730231 | 25.81821 | 2.421471 |
| 13    | 0.023469 | 0.034919           | 4.158704 | 18.91613 | 2.357453 |
| 14    | 0.023156 | 0.027911           | 5.207715 | 31.06376 | 2.227863 |
| 15    | 0.019708 | 0.014085           | 4.763091 | 25.00937 | 2.178213 |

Table 5.3 and 5.4 shows the feature values obtained from the Pancreatic Cell tumor images of test sample of benign and malignant respectively. These two tables show only 100 images of both (50 benign and 50 malignant image) cases of the pancreatic tumor particularly CT scan images. For this application of segmentation of tumor cells many features are suitable. Here suitable features like contrast, cluster prominence, cluster shade, correlation, energy and homogeneity are extracted for the apparent classification and identification of disease in the database images.

### Classification of Red Pancreatic Cell Tumour CT Scan

#### Database Images

In this section the sample images are classified by DNN, SVM, KNN, BRT, CNN, ANN and Deep learning classifier. It classifies the cancerous image, whether the region has benign lung or malignant lung image. ResNet-50 inception synergic network classifier classifies the tumor CT images and provides better accuracy. The achieved accuracy is 99.231%. The performances are analyzed based on the sensitivity, specificity, precision, accuracy, error value. Finally, above mentioned classifier performances are compared and noticed deep learning where the performance is found to be best. For comparison, confusion matrix and ROC curve are plotted for above classifiers.

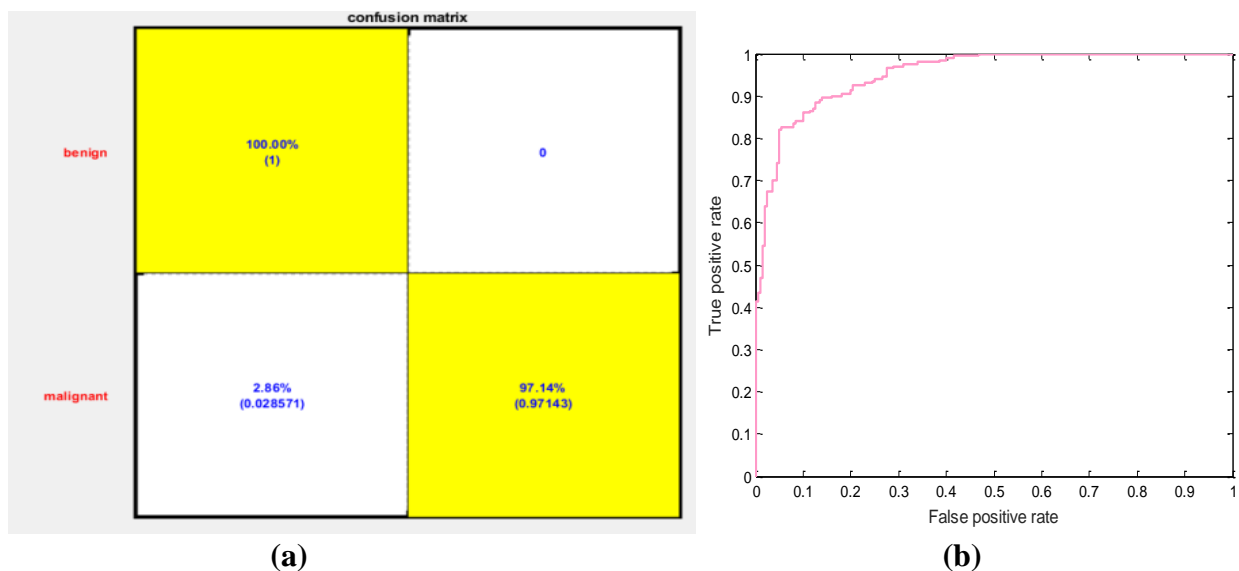
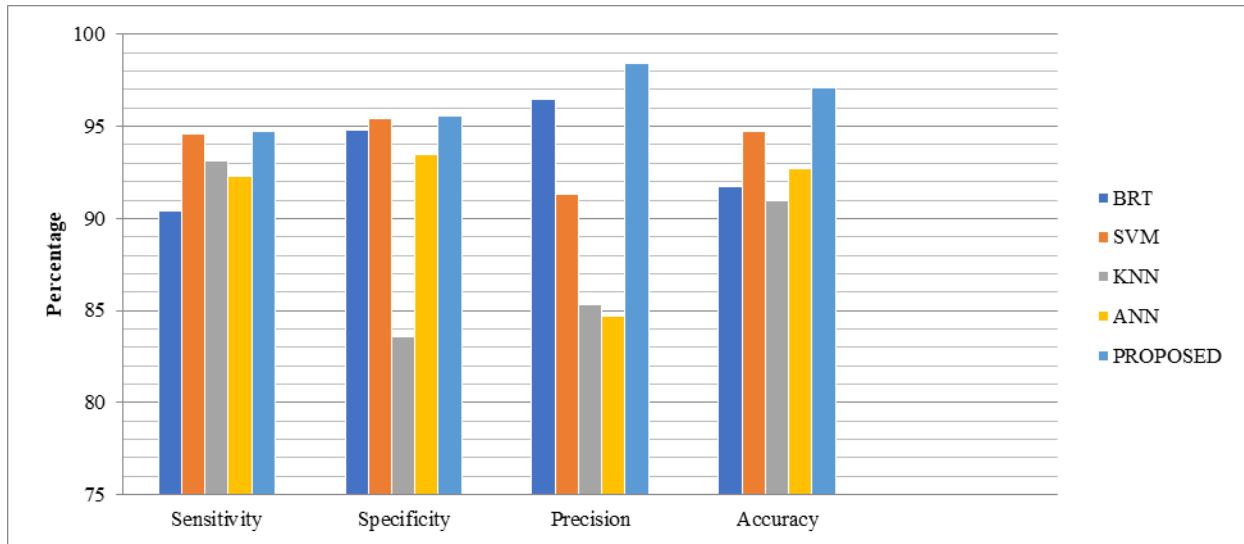


Figure 5.4 Classifier outputs obtained using Deep Learning classifier: a) Confusion matrix, b) ROC Curve

In Figure 5.4(a) Class 0 indicates benign Red Pancreatic Cell tumor CT scan image and Class 1 indicates malignant Pancreatic Cell tumor CT scan image. Deep learning classifier with Histogram based features, 50 of the total 50 benign cases are correctly classified as

benign (TP), while none of them are misclassified as malignant (FN). 48 of the 50 malignant cases used for testing are correctly classified as malignant (TN), while 2 of them are misclassified as benign (FP). Deep learning confusion matrix, TPs percentage is 48.5%, FPs percentage is 51.5%, FNs percentage is 64.9% and TNs percentage is 35.1%. The accuracy of Deep learning classifier is 97.1%. The rate of misclassification is 2.9%.



**Figure 5.5 Comparisons of Error values with different classifier**

Figure.5.5 shows the graphical representation of comparison of sensitivity, specificity, precision, accuracy values of different classification techniques applied on pancreatic tumor CT images. X-axis represents the various parameters of different classifiers and Y-axis represents the values in terms of percentage by the classification techniques.

## Conclusion

This conclusion discussed the results and comparative analysis of Red Pancreatic Cell cancer CT scan database images with various classifiers. The PCCD database of pancreatic cancer images are used in this work. Color Conversion and Anisolateral filter are used as a preprocessing method which is applied on the database image. Tumor regions are segmented using FK-NNE Segmentation and Semantic Segmentation methods and Histogram based features are extracted. Finally, the Pancreatic Cell tumor image are classified whether it benign or malignant image using ResNet-50 inceptive synergic network classifier. Performance of classifier is analyzed based on the sensitivity, specificity, precision, error value and accuracy. The proposed method of ResNet-50 inceptive synergic network classifier is compared with SVM, KNN, BRT, ANN, Deep Learning classifiers. For each classifier, confusion matrix and ROC curve are plotted. ResNet-50 inceptive synergic network classifier provides 99.32% accuracy.

## References

- Chang, H., Borowsky, A., Spellman, P., & Parvin, B. (2013). Classification of tumor histology via morphometric context. *In Proceedings of the IEEE Conference on Computer Vision and Pattern Recognition*, 2203-2210.
- Hussein, N.J., Hu, F., & He, F. (2017). Multisensor of thermal and visual images to detect concealed weapon using harmony search image fusion approach. *Pattern Recognition Letters*, 94, 219-227.
- Gurcan, M.N., Boucheron, L.E., Can, A., Madabhushi, A., Rajpoot, N.M., & Yener, B. (2009). Histopathological image analysis: A review. *IEEE reviews in biomedical engineering*, 2, 147-171.
- Jiang, H., Zhao, D., Zheng, R., & Ma, X. (2015). Construction of pancreatic cancer classifier based on SVM optimized by improved FOA. *BioMed research international*.
- Pahari, P., Basak, P., & Sarkar, A. (2017). Biomarker detection on Pancreatic cancer dataset using entropy based spectral clustering. *In 2017 Third International Conference on Research in Computational Intelligence and Communication Networks (ICRCICN)*, 208-212.
- Reddy, C.K.K., Raju, G.V S., & Anisha, P.R. (2015). Detection of pancreatic cancer using clustering and wavelet transform techniques. *In International Conference on Computational Intelligence and Communication Networks (CICN)*, 332-336.
- Zhou, Y., Chang, H., Barner, K., Spellman, P., & Parvin, B. (2014). Classification of histology sections via multispectral convolutional sparse coding. *In Proceedings of the IEEE Conference on Computer Vision and Pattern Recognition*, 3081-3088.
- Zhou, J., & Troyanskaya, O.G. (2015). Predicting effects of noncoding variants with deep learning-based sequence model. *Nature methods*, 12(10), 931-934.
- Moschopoulos, C., Popovic, D., Sifrim, A., Beligiannis, G., De Moor, B., & Moreau, Y. (2013). A genetic algorithm for pancreatic cancer diagnosis. *In International conference on engineering applications of neural networks, Springer, Berlin, Heidelberg*, 222-230.
- Xu, Y., Zhu, J.Y., Eric, I., Chang, C., Lai, M., & Tu, Z. (2014). Weakly supervised histopathology cancer image segmentation and classification. *Medical image analysis*, 18(3), 591-604.
- Wang, J., Yang, X., Cai, H., Tan, W., Jin, C., & Li, L. (2016). Discrimination of breast cancer with microcalcifications on mammography by deep learning. *Scientific reports*, 6(1), 1-9.
- Zhang, D., Zhang, J., Zhang, Q., Han, J., Zhang, S., & Han, J. (2021). Automatic pancreas segmentation based on lightweight DCNN modules and spatial prior propagation. *Pattern Recognition*, 114, 107762.
- Hussein, N.J., Hu, F., He, F., & Ayoob, A.A. (2016). Enhancing the seismic histogram equalization of multi-fusion for infrared image of concealed weapon detection. *International Conference on Innovative Material Science and Technology*.
- Liu, L., Cheng, J., Quan, Q., Wu, F.X., Wang, Y.P., & Wang, J. (2020). A survey on U-shaped networks in medical image segmentations. *Neurocomputing*, 409, 244-258.

- Shi, Y., Gao, F., Qi, Y., Lu, H., Ai, F., Hou, Y., & Cai, X. (2020). Computed tomography-adjusted fistula risk score for predicting clinically relevant postoperative pancreatic fistula after pancreatoduodenectomy: Training and external validation of model upgrade. *EBioMedicine*, 62, 103096.
- Haque, I.R.I., & Neubert, J. (2020). Deep learning approaches to biomedical image segmentation. *Informatics in Medicine Unlocked*, 18, 100297.
- Kurbanov, S.K., & Beknazarova, S.S. (2020). Deep learning approaches to biomedical image segmentation.
- Chen, X., Hu, Y., Zhang, Z., Wang, B., Zhang, L., Shi, F., & Jiang, X. (2019). A graph-based approach to automated EUS image layer segmentation and abnormal region detection. *Neurocomputing*, 336, 79-91.
- Hussein, N.J. (2020). Robust Iris Recognition Framework Using Computer Vision Algorithms. *In 2020 4th International Conference on Smart Grid and Smart Cities (ICSGSC)*, 101-108.
- Loi, S., Mori, M., Benedetti, G., Partelli, S., Broggi, S., Cattaneo, G. M., & Fiorino, C. (2020). Robustness of CT radiomic features against image discretization and interpolation in characterizing pancreatic neuroendocrine neoplasms. *Physica Medica*, 76, 125-133.
- Saito, A., Nawano, S., & Shimizu, A. (2016). Joint optimization of segmentation and shape prior from level-set-based statistical shape model, and its application to the automated segmentation of abdominal organs. *Medical image analysis*, 28, 46-65.
- van der Meulen, T., Mawla, A.M., DiGruccio, M.R., Adams, M.W., Nies, V., Dólleman, S., & Huisin, M.O. (2017). Virgin beta cells persist throughout life at a neogenic niche within pancreatic islets. *Cell metabolism*, 25(4), 911-926.
- Rosow, D.E., Liss, A.S., Strobel, O., Fritz, S., Bausch, D., Valsangkar, N.P., & Thayer, S.P. (2012). Sonic Hedgehog in pancreatic cancer: from bench to bedside, then back to the bench. *Surgery*, 152(3), S19-S32.
- Hussein, N.J. (2020). Clarifying Image Tumor of Early Breast Cancer Detection Using Monogamy Imaging. *International Journal of Advanced Science and Technology*, 29(3s), 97-103.